Resistive switching in a LaMnO3+δ / TiN memory cell investigated by operando hard X-ray photoelectron spectroscopy

Benjamin Meunier, Eugenie Martinez, Raquel Rodriguez-Lamas, Dolors Pla, Mónica Burriel, Michel Boudard, Carmen Jimenez, Jean-Pascal Rueff, Olivier Renault

Resistive switching in a $LaMnO_{3+\delta}$/TiN memory cell investigated by *operando* hard X-ray photoelectron spectroscopy

Benjamin Meunier[1], Eugénie Martinez[2], Raquel Rodriguez-Lamas[1], Dolors Pla[1], Monica Burriel[1], Michel Boudard[1], Carmen Jimenez[1], Jean-Pascal Rueff[3,4], Olivier Renault[2]

[1]Univ. Grenoble Alpes, CNRS, Grenoble INP*, LMGP, F-38000 Grenoble, France

* *Institute of Engineering Univ. Grenoble Alpes*

[2]Univ. Grenoble Alpes, CEA, LETI, 38000 Grenoble, France

[3]Synchrotron-SOLEIL, BP 48, Saint-Aubin, F-91192 Gif-sur-Yvette, France

[4]Sorbonne Université, CNRS, Laboratoire de Chimie Physique - Matière et Rayonnement (LCPMR), F-75005 Paris, France

ABSTRACT

Transition metal oxides are promising candidates in the development of valence change memories thanks to their ability to present valence change mechanism. The resistive switching mechanism of TiN/$LaMnO_{3+\delta}$/Pt devices was investigated by *operando* hard X-ray photoelectron spectroscopy after careful *in situ* electrical characterization. The results presented here highlight the oxygen exchange process at the TiN/LMO interface. The active TiN top electrode acts as an oxygen getter, pumping O^{2-} anions which are attracted by the positive bias and repelling them under negative bias. This drift of charged defects is correlated with variations of the interfacial resistance. Our results confirm the critical role of the TiN/LMO interface as well as of oxygen drift in the resistive switching behaviour of such devices.

Motivated by the growing interest in novel non-volatile resistive random-access memories (RRAMs), many new oxide-based heterostructures have emerged as potential candidates to build alternative memristive devices. Among the plethora of oxides exhibiting valence change mechanism, a number of perovskites, such as (Pr,Ca)MnO_3,[1] $SmNiO_3$,[2] $SrZrO_3$,[3-5] $LaSrMnO_3$,[6] as well as the thoroughly-studied $SrTiO_3$[7] have shown memristive behavior. Despite their promising functional properties (high speed, large ON/OFF ratio, large programming window, high endurance), fundamental knowledge and a thorough understanding of the RS mechanisms involved are in most cases still rather scarce. This is due to the difficulty to get element-specific information from the resistive material in an operating device.

The non-stoichiometric transition metal oxide $LaMnO_{3+\delta}$ (LMO) shows a resistive switching behavior which was shown to be governed by the oxygen vacancy content of the material.[8,9] The apparent oxygen excess in LMO is ascribed to the formation of La and/or Mn cation vacancy sites (i.e. $La_{1-x}\square_x Mn_{1-y}\square_y O_3$, *viz.* $LaMnO_{3+\delta}$), where □ represents cation vacancies and charge neutrality remains fulfilled thanks to the coexistence of Mn^{3+}/Mn^{4+} oxidation states.[10-13] Therefore, the valence state of the material is strongly correlated to the oxygen content and Mn4+ can be seen as a dopant.[14]

We recently investigated the microscopic mechanisms of local interfacial RS in $LaMnO_{3+\delta}$ by conductive atomic force microscopy (c-AFM)[15] and highlighted that the change in resistance is associated with a drift of oxygen ions to the surface and the concomitant variation in the Mn valence state, which results in modifications in the transport mechanism. However, the configuration used presents several specificities (*e.g.* low current density, bare surface, large active area …) that do not match the requirements of a standard functional device. Thus, to go a step further in the understanding of the memristive behavior of LMO-based cells, we have now tested more realistic operating devices, in which the active oxide layer is sandwiched between a top- and a bottom-electrode.

Hard x-ray photoelectron spectroscopy (HAXPES) has shown excellent capabilities for non-destructive *operando* characterization of functional devices.[16-18] Indeed, compared to conventional XPS with laboratory AlKα (1486.6 eV) or MgKα (1253.6 eV) sources, the use of hard x-ray

synchrotron radiation (2.4 – 12 keV) gives information from a region up to 5 times deeper inside the sample and even deeper using inelastic background analysis.[19,20] HAXPES has been successfully implemented during resistive switching operation to study buried interfaces of different oxide-based heterostructures such as Ti/HfO_x,[21-26] TiN/$Hf_{0.5}Zr_{0.5}O_2$,[27] Pt/Ti/$Pr_{0.5}Ca_{0.5}MnO_3$,[22] Au/FeSTO/NbSTO,[28] and TiN/Pt/NiO.[29] Real *operando* measurements, consisting in biasing the device while performing HAXPES, are therefore enlightening in order to understand the changes in elemental composition and charge distribution inside the device. Such a method was previously used for studying interface polarization in piezoelectric oxide-based high-density capacitors.[30]

In the present contribution, we study the case of LMO memristive devices grown on platinized silicon and covered by TiN, a technologically-relevant top electrode. Operando HAXPES measurements were performed at different resistance states, carefully induced by in situ electrical characterization. The results reveal the chemical modifications and reactions occurring at the LMO/TiN interface.

In order to match the HAXPES requirements, the TiN electrode should be thin enough to allow the photoelectrons passing through and the remote electrical contacts should be employed to avoid any obstruction of the active area. The resulting design is presented in **Figure 1** (a). The LMO thin film (100 nm-thick, grown following strategy III of Ref.[31]) is partially covered by a 50 nm thick Si_3N_4 insulating layer deposited by sputtering (CT100 Alliance Concept). The structural characterization of the LMO film (XRD and Raman spectroscopy) exhibiting the coexistence of both rhombohedral and orthorhombic phases can be found in **Figure S2** of the **Supporting Information**. 100x100 μm² squared craters were etched through the Si_3N_4 layer and subsequently covered by a TiN layer of approximately 6 nm thick also deposited by sputtering. In this way, the HAXPES measurements were carried out on well-defined regions of interest of 100×100 μm² comprising the top TiN top electrode and the LMO surface below, simultaneously achieving the electrical biasing of the sample. 100 nm-thick gold current collectors were then deposited onto the Si_3N_4, directly contacting the TiN top

electrode and allowing the wire bonding to the sample holder. As shown in Figure 1(b) the sample holder is a printed circuit board hosting several electrodes. The grounded electrode (left of the image) is wire-bonded to the Pt bottom electrode, while the four top electrodes (right of the image) are wire-bonded to the top Au/TiN electrodes and each of them can be independently connected to a sourcemeter (Keithley 2635B). Due to the large distance between the sample in the HAXPES chamber and the operator, the wire resistance and multiple contacts resistance cannot be neglected. The difference between the resistance measured directly at the sample's output and the resistance once the sample is mounted and placed in the HAXPES chamber give a total external resistance of 2.9 Ω.

The HAXPES experiments were performed at the Galaxies beamline, SOLEIL synchrotron facility (St-Aubin, France). The pressure in the analysis chamber remained around 10^{-8}-10^{-7} mbar during the whole experiment. The photon energy was set to 7994.51 eV (as determined from the Fermi level of the Au top electrode at zero bias) with a take-off angle of 50°. The incident photon energy was selected with a Si(333) double crystal monochromator, and the photons were focused to a 30×80 μm^2 beam spot using a toroidal mirror. The photon and analyzer bandwidths were both set to 150 meV providing an overall energy resolution of 210 meV. The Au 4f, Ti 1s and O 1s core-levels were recorded after each change in resistance, while still biasing the sample. The La 3d core-level could not be recorded due to the poor signal-to-noise ratio and the large energy range required, while the manganese core-levels were not analyzed because of intrinsically low cross-sections and severe overlapping with the Au photoemission lines. A Shirley-type background was subtracted from all the spectra. The inelastic mean free path estimated for the different core levels through the LMO/TiN stack provides an average sampling depth of 25 nm.[32]

The initial spectra (at 0 V and initial resistance state - IRS) of Ti 1s and O 1s are shown in Figure 2(c) and (d). Peak fitting was performed using a pseudo-Voigt function with 70% and 20 % of Lorentzian peak for Ti 1s and O 1s respectively. The Ti 1s photoemission spectrum consists of three contributions. The component at the lowest binding energy (4965.6 eV) corresponds to bulk TiN while the two other

contributions are attributed to TiO_xN_y (4966.6 eV) and TiO_x (4968.2 eV) resulting from the oxidation of TiN.[33,34] The larger width of the oxide peaks (FWHM = 2.6 eV) compared to the TiN peak (FWHM = 1.3 eV) is attributed to inhomogeneities in the oxides composition. The composition of the top as-deposited electrode has been calculated to be of 32% TiN and 68% of oxides (26% TiO_xN_y and 42% TiO_x). Even if the fully oxidized TiO_x is more likely to be found on the surface and TiO_xN_y at the interface, these considerations are not fully accurate regarding the low thickness of the top electrode.

The O 1s spectrum in Figure 2(d) is dominated by the SiO_2 contribution coming from the Si_3N_4 oxidized surface due to the large footprint of the incident beam on the surface. Two other contributions are identified at 530.6 eV and 530.3 eV assigned to Ti-O bonds (from TiO_x and TiO_xN_y) and to LMO, respectively. A more complete HAXPES characterization of the sample (presenting La $3d_{3/2}$, Mn 3s, O 1s and N 1s in different regions) can be found in **Figure S3** of **Supporting Information**.

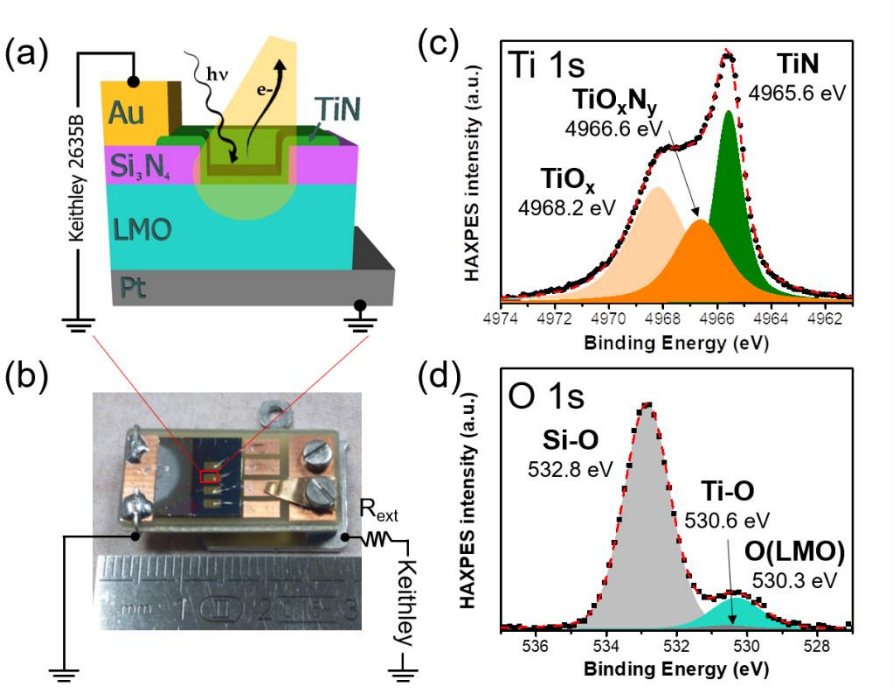

Figure 1 *(a) sample description (b) picture of a mounted sample (c)(d)HAXPES spectra of Ti 1s and O 1s for the stack $TiO_x/TiN/TiO_xN_y/LaMnO_{3+\delta}$ in the initial resistance state at 0V.*

We now address the results of the *operando* measurements of the LMO/TiN memory cell. The Au 4f, O 1s and Ti 1s core-levels were recorded while biasing the device with different voltages following the sequence: 0 V → 2.5 V → 5V → -2.5V → -5V → 0V. The core level spectra for each step are presented in the **Supporting Information** (Au 4f in **Figure S4**, Ti 1s in **Figure S5** and O 1s in **Figure S6**). It should be notice that the -5V and final 0V spectra are similar shape which exclude the presence of potential volatile effects due to the presence of the electric field. During this sequence, the sample resistance changes from the initial resistance state (R= 6.2 Ω) to the HRS (R= 52 Ω) at +5 V and back to a LRS (R=12 Ω) at -5 V.

Figure 2(a) and (b) show the peak shifts, relative to 0 bias, of Au 4f, Ti 1s(TiN), O 1s(LMO) and O 1s(Ti-O) for different applied voltages and resistance states. When a bias is applied, the energy levels will drift away from the Fermi level and the measured kinetic energy of electrons will be shifted. The energy shift of an element corresponds to the voltage "seen" at the location of this element in the device. Thus, as depicted in Figure 3(b) the deeper the layer, the smaller the corresponding HAXPES shift (i.e. $V_{Au} > V_{TiN} > V_{LMO}$). The voltage applied to the device is progressively lost in the series resistances corresponding to each material or interface of the stack. Considering the Au 4f peak from the top electrode, the total resistance ($R_{tot}=R_{dev}+R_{ext}$) of the device ($R_{dev} = R_{LMO}+R_{TiN}+R_{Au}$) and the external resistance ($V_{appl} - V_{Au} = I.R_{ext}$) can be calculated with the following potential divider relationship:

$$R_{tot} = R_{ext}.(1 + \frac{V_{Au}}{V_{appl} - V_{Au}})$$

being R_{ext} = 2.9 Ω the external resistance and V_{appl} the applied voltage. Therefore, for V_{appl} = +5 V, the Au 4f energy shift yields V_{Au} = 4.73 V and the total resistance drop can be calculated to be R_{tot} = 53.7 Ω, meaning that the device is in HRS. Similarly, for V_{appl} = -5 V, V_{Au} = -1.0 V and R_{tot} = 3.6 Ω, corresponding to the LRS case. These resistance values are comparable with those experimentally measured with the Keithley during the HAXPES measurement (R_{HRS} = 52 Ω and R_{LRS} = 12 Ω), the differences in LRS being due to leakage current inside the material. This highlights the good

reliability of the experimental set-up and the relevance of the spectroscopic measurements in a specific resistance state of the device. When switching the device to HRS, *i.e.* when applying a positive bias (2.5 and 5 V), a potential drop is observed between the TiN and LMO layers and between the TiN and Au electrode. During the RESET event (IRS to HRS) voltage difference between each layer increase, first between TiN and LMO at 2.5 V and then between TiN and Au. During the SET event (HRS to LRS) at -2.5 V the potential drop between TiN and LMO strongly decreases (i.e. V_{TiN}-V_{LMO} ~ 0 V) to almost reach the same voltage.

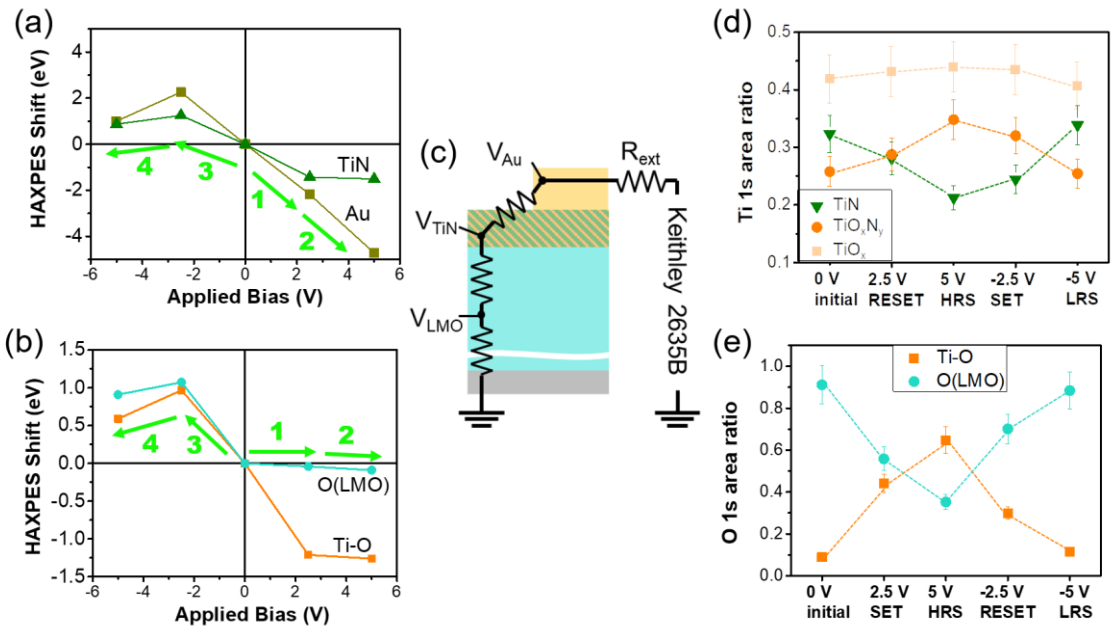

Figure 2. *(a) HAXPES shift of Au 4f, Ti 1s and (b) O 1s depending on the applied voltage (c) equivalent circuit of the structure with R_{ext} = 2.9 Ω (d) relative areas of all Ti 1s and (e) O 1s contributions depending on the applied bias and the resistance state*

Figure 2(c) shows the evolution of all Ti components after normalization of their area by the total Ti 1s area (which is assumed to be constant). During the RESET event (from 0 V to 5 V), the Ti 1s area from TiN decreases while the oxide contributions increase indicating the oxidation of the positively biased TiN electrode. Similar behavior of the Ti-O is observed in the O 1s spectra in Figure S5 as well as a decrease of the O(LMO) contribution. Comparing each of the Ti oxide, the TiO_xN_y (partially oxidized TiN) ratio rises from 26% to 36% while the TiO_x (fully oxidized TiN) ratio only rises from

42% to 44%. This is indicative of the partial oxidation of the TiN electrode, remaining moderate during the RESET event. This oxygen drift from the LMO to the top electrode, in the form of O^{2-} anions, is driven by the electric field. Conversely, during the SET event (applying -2.5 and -5 V), each contribution goes back to a value close to its initial value. A reversed oxygen drift, from TiO_xN_y back into the LMO is observed driven by the electric field.

The consequence of this redox reaction at the interfacial TiO_xN_y layer is the increase/decrease of the potential drop previously observed at this interface. The exchange of oxygen ions between LMO and the TiN electrode is described in **Figure 3**.

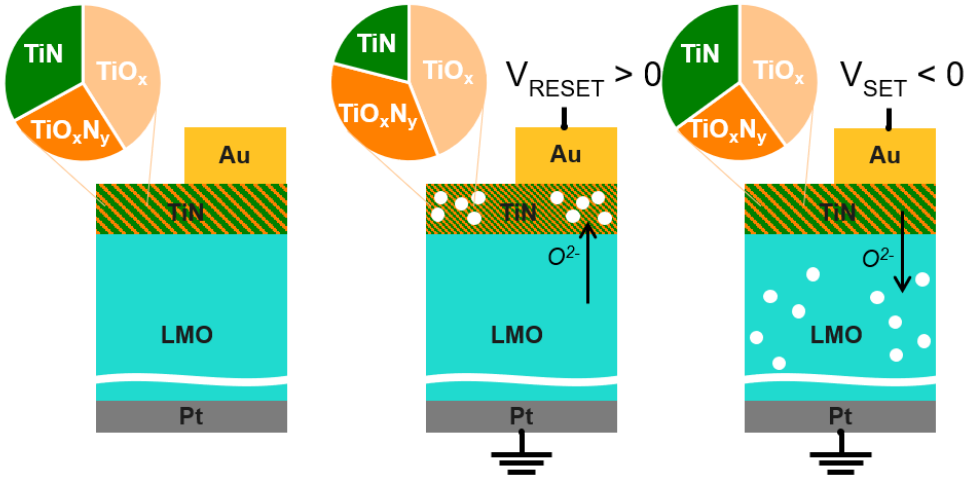

Figure 3. *Sketch of the proposed oxygen exchange process occurring during RESET ($V_{SET} > 0$) and SET ($V_{RESET} < 0$). Inserts: the nominal composition of the TiN electrode based on the quantification of the Ti 1s area ratios shown in Figure3(c).*

In this work we presented *operando* HAXPES measurements for investigating the resistive switching mechanisms taking place in a TiN/LMO/Pt memory cell under application of electrical bias. The use of HAXPES has successfully demonstrated its ability to observe buried interfaces and fingerprint relevant modifications occurring during resistive switching. In particular, spectra recorded during the process reveal changes in the composition of both the TiN electrode and the LMO itself. Fitting of the Ti 1s spectra (and confirmed by the O 1s spectra) clearly indicates a partial oxidation of the TiN electrode and reduction of LMO surface during RESET followed by the reverse reactions during SET.

The mechanism can be described by a redox reaction triggered by the oxygen drift at the TiN/LMO interface due to the external bias. The TiO_xN_y interlayer plays the role of an oxygen getter during RESET, expelling oxygen back in LMO during the SET process. Thanks to careful *operando* spectroscopic analysis, we proposed a redox model to fully describe the physiochemical mechanism occurring in a potential technologically-relevant memory cell consisting in a $LaMnO_{3+\delta}$ active layer and a TiN top electrode.

SUPPORTING INFORMATION

See supporting information for more complete sample characterization and further detailed HAXPES spectra.

ACKNOWLEDGMENTS

This work has been supported by the ANR funded project "Alps Memories" (ANR-15-CE24-0018). We acknowledge SOLEIL for provision of synchrotron radiation facilities (Proposal No. 20170169). The authors want to thank Odette Chaix-Pluchery and Hervé Roussel for Raman and X-ray diffraction measurements. Sample fabrication has been performed with the help of the "Plateforme Technologique Amont" of Grenoble with the financial support of the CNRS Renatech network. In addition, this work benefited from the facilities and expertise of the OPE)N(RA characterization platform of FMNT (FR 2542, fmnt.fr) supported by CNRS, Grenoble INP and UGA.

REFERENCES

[1] D. S. Kim, Y. H. Kim, C. E. Lee, Y. T. Kim, *Phys. Rev. B* **2006**, 74, 174430.

[2] J. Shi, S. D. Ha, Y. Zhou, F. Schoofs, S. Ramanathan, *Nat. Commun.* **2013**, 4, 2676.

[3] L. Weston, A. Janotti, X. Y. Cui, B. Himmetoglu, C. Stampfl, C.G. Van de Walle, *Phys. Rev. B* **2015**, 92, 085201.

[4] D. S. Kim, C. E. Lee, Y. H. Kim, Y. Y. Kim, *J. Appl. Phys.* **2006**, 100(9), 0-4.

[5] S. Q. Liu, N. J. Wu, A. Ignatiev, *Appl. Phys. Lett.* **2000**, 76, 2749.

[6] J. C. Gonzalez-Rosillo, R. Ortega-Hernandez, J. Jareño-Cerulla, E. Miranda, J. Suñe, X. Granados, X. Obradors, A. Palau, T. Puig, *J. Elecrtoceram.* **2017**, 39, 185.

[7] K. Szot, W. Speier, G. Bihlmayer, R. Waser, *Nat. Mater.* **2006**, 5, 312-320.

[8] Y.-L. Jin, Z.-T. Xu, K.-J. Jin, C. Ge, H.B. Lu, G.-Z. Yang, *Mod. Phys. Lett. B* **2013**, 27(11), 1350074.

[9] Z.-T. Xu, K.-J. Jin, L. Gu, Y.-L. Jin, C. Ge, C. Wang, H.-Z. Guo, H.-B. Lu, R.-Q. Zhao, G.-Z. Yang, *Small* **2012**, 8, 1279-1284.

[10] J. Töpfer, J. B. Goodenough, *J. Solid State Chem.* **1997**, 130, 117-128.

[11] B. C. Tofield, W. R. Scott, *J. Solid State Chem.* **1974**, 10, 183-194.

[12] J. A. M. van Roosmalen, E. H. P. Cordfunke, *J. Solid State Chem.* **1994**, 110, 106-108.

[13] J. A. M. van Roosmalen, P. van Vlaanderen, E. H. P. Cordfunke, *J. Solid State Chem.* **1995**, 114, 516-523.

[14] S. Badgevicius, K. Maas, M. Boudard, M. Burriel, *J. Electroceram.* **2017**, 39, 157.

[15] B. Meunier, D. Pla, R. Rodriguez-Lamas, M. Boudard, O. Chaix-Pluchery, E. Martinez, N. Chevalier, C. Jiménez, M. Burriel, O. Renault, ACS Appl. Electron. Mater. **2019**, 1, 5, 675-683.

[16] F. Borgatti, F. Offi, P. Torelli, G. Monaco, G. Panaccione, *J. Electron. Spectrosc.* **2013**, 190, 228-234.

[17] D. Céolin, J. M. Ablett, D. Prieur, T. Moreno, J.-P. Rueff, T. Marchenko, L. Journel, R. Guillemin, B. Pilette, T. Marin, M. Simon, *J. Electron. Spectrosc.* **2013**, 190, 188-192.

[18] J. Rubio-Zuazo, G. R. Castro, *J. Electron. Spectrosc.* **2013**, 190, 205-209.

[19] S. Tougaard, *Surf. Interface Anal.* **1998**, 26(4), 249-269.

[20] S. Tougaard, *J. Electron. Spectrosc. Relat. Phenom.* **2010**, 178-179, 128-153.

[21] T. Bertaud, M. Sowinska, D. Walczyk, S. Thiess, A. Gloskovskii, C. Walczyk, T. Shroeder, *Appl. Phys. Lett.* **2012**, 101, 143501.

[22] F. Borgatti, C. Park, A. Herpers, F. Offi, R. Egoavil, Y. Yamashita, A. Yang, M. Kobata, K. Kobayashi, J. Verbeek, G. Panaccione, R. Dittmann, *Nanoscale* **2013**, 5, 3954.

[23] Y. S. Lin, F. Zeng, S. G. Tang, H. Y. Liu, C. Chen, S. Gao, Y. G. Wang, F. Pan, *J. Appl. Phys.* **2013**, 113, 164510.

[24] S. U. Sharath, T. Bertaud, J. Kurian, E. Hildebrandt, C. Walczyk, P. Calka, P. Zaumseil, M. Sowinska, D. Walczyk, A. Gloskovskii, T. Schroeder, L. Alff, *Appl. Phys. Lett.* **2014**, 104, 063502.

[25] M. Sowinska, T. Bertaud, D. Walczyk, S. Thiess, M. A. Schubert, *Appl. Phys. Lett.* **2012**, 100, 233509.

[26] M. Sowinska, T. Bertaud, D. Walczyk, S. Thiess, P. Calka, L. Alff, C. Walczyk, T. Schroeder, *J. Appl. Phys.* **2014**, 115, 204509.

[27] Y. Matveyev, D. Negrov, A. Chernikova, Y. Lebedinskii, R. Kirtaev, S. Zarubin, E. Suvorova, A. Gloskovskii, A. Zenkevich, *ACS Appl. Mater. Interfaces* **2017**, 9, 43370-43376.

[28] C. Lenser, A. Koehl, I. Slipukhina, H. Du, M. Patt, V. Feyer, C. M. Schneider, M. Lezaic, R. Waser, R. Dittmann, *Adv. Funct. Mater.* **2015**, 25, 6360-6368.

[29] P. Calka, E. Martinez, D. Lafond, S. Minoret, S. Tirano, B. Detlefs, J. Roy, J. Zegenhagen, C. Guedj, *J. Appl. Phys.* **2011**, 109, 124507.

[30] I. Gueye, G. Le Rhum, O. Renault, D. Cooper, D. Ceolin, J.-P. Rueff, N. Barrett, *Appl. Phys. Lett.* **2017**, 11(3), 032906.

[31] R. Rodriguez-Lamas, D. Pla, O. Chaix-Pluchery, B. Meunier, F. Wilhelm, A. Rogalev, L. Rapenne, X. Mescot, Q. Rafhay, H. Roussel, M. Boudard, C. Jiménez, M. Burriel, *Beilstein J. Nanotech.* **2018**, 10, 389-398.

[32] H. Shinotsuka, S. Tanuma, C. J. Powell, and D. R. Penn, Surf. Interface Anal. 47, 871 (2015).

[33] O. Renault, E. Martinez, C. Zborowski, J. Mann, R. Inoue, J. Newman, K. Watanabe, *Surf. Interface Anal.* **2018**,1-5.

[34] P. Risterucci, O. Renault, C. Zborowski, D. Bertrand, E. Torres, J.-P. Rueff, D. Ceolin, G. Grenet, S. Tougaard, *Appl. Surf. Sci,* **2017**, 402, 78-85.